International Journal of Offshore and Polar Engineering (ISSN 1053-5381)

Vol. 36, No. 2, June 2026, pp. 162–171; https://doi.org/10.17736/ijope.2026.ak82

http://www.isope.org/publications

Effect of Density Stratification on a Self-Propelled Generic Submarine near the Free Surface

Linjie Li, Liushuai Cao* and Decheng Wan*†
Computational Marine Hydrodynamics Lab (CMHL), School of Ocean and Civil Engineering
Shanghai Jiao Tong University, Shanghai, China

Fuchang Zhou
Wuhan Second Ship Design and Research Institute
Wuhan, China

Jian Zhang
Ningbo Pilot Station, Ningbo Dagang Pilotage Co., Ltd.
Ningbo, China

A self-propelled Joubert BB2 submarine operating near the free surface was investigated in three fluid environments: homogeneous, strongly stratified, and linearly stratified. The differences in flow fields under various submergence conditions were analyzed. The results show that density stratification has only a minor effect on propeller rotational speed and thrust, with deviations within 3%. When the submarine operates close to the free surface, the flow-field characteristics are nearly identical among the three fluids. However, with increasing submergence depth, the differences in wake disturbances between the stratified and homogeneous fluids become more pronounced. Specifically, the vertical velocity along the submarine axis downstream decreases by 38.7% and 61.9% in the strongly and linearly stratified cases, respectively. Under such conditions, the influence of density stratification cannot be neglected.

INTRODUCTION

It is well known that submarines traveling under the free surface are subject to greater drag as well as lift and pitching moments relative to deep-water environments. Amiri et al. (2018) investigated how the free surface affects the hydrodynamics of a shallowly submerged submarine, and Sudharsun et al. (2022) investigated Bernoulli's hump for submarines moving underwater. Dong et al. (2022) investigated the hydrodynamic performance of a submarine navigating near the free surface with long-crested waves, analyzing the effects of irregular waves and underwater depth. However, the effect of propeller rotation on the flow field was not considered in these studies.

Numerous studies on self-propulsion have been conducted using the DARPA Suboff geometry. Liefvendahl and Troëng (2011) used LES to study the periodic variation of propeller blade loads on a submarine. Chase and Carrica (2013) simulated the application of a submarine propeller for self-propulsion and showed that the same method when applied to surface ships can be used to calculate the self-propulsion of a submarine. Sezen et al. (2018) used the RANS method to study self-propulsion of Suboff and found that the body force method estimated lower propulsive efficiency and higher transferred power, while the hull was more efficient. Lungu (2022) studied the numerical simulation of self-propelled Suboff working in deep water and near free surface based on DES, revealing the free surface working regimes.

Unlike the slender hull structure of the Suboff submarine, the Joubert BB2, a generic submarine, is shorter and fatter. Li et al. (2015) first put forward the effects of the free surface on the performance of the Joubert BB2 submarine with a propeller, showing that operating closer to the water surface resulted in higher propeller loads and lower efficiency. Carrica et al. (2019) comparatively analyzed submarine self-propulsion in calm water and waves and found that hull/free surface interactions lead to wake fluctuations. Guo et al. (2024) conducted an investigation into the steady turning motion of a Joubert BB2 submarine near the free surface, comprehensively analyzing how variations in submerged depth and forward speed jointly affect the submarine's maneuverability.

The effect of density stratification on submarine self-propulsion has not been considered in the above studies, while the density of seawater varies along the depth direction in the actual ocean due to temperature, salinity, and other factors. There have been some studies considering the effect of density stratification on the submarine hydrodynamics wake. Ma et al. (2019) studied the internal and free surface waves induced by the Suboff in a strongly stratified fluid. Huang et al. (2022) compared and analyzed the difference between the wake and free surface characteristics of the Joubert BB2 submarine in a homogeneous and linearly stratified fluid. Cao et al. (2023) numerically simulated the hydrodynamic performance and wake of Suboff in continuously stratified fluid. However, these studies still simulated the fixed speed of a submarine by the incoming flow method but did not account for the rotation of the propeller.

From the above studies, it is evident that research on self-propelled submarines with propellers has not yet considered the effects of density stratification, while studies on density-stratified

* ISOPE Member; † Corresponding author.
Received July 26, 2025; updated and further revised manuscript received by the editors December 1, 2025. The original version (prior to the final updated and revised manuscript) was presented at the Thirty-fifth International Ocean and Polar Engineering Conference (ISOPE-2025), Goyang/Seoul, Korea, June 1–6, 2025.
KEY WORDS: Submarine, self-propulsion, stratified fluid, wakes, free surface.

fluid have generally neglected propeller rotation. Therefore, the present work combines these two aspects by considering the influence of density stratification on a self-propelled generic submarine operating near the free surface. All numerical simulations in this study were carried out using STAR-CCM+.

NUMERICAL METHODS

Governing Equations

In this paper, in addition to the continuity and momentum equations under the Boussinesq approximation, the heat equation is also solved in the numerical simulation of the linear density-stratified fluid (Cao et al., 2021), and the governing equations are shown in Eq. 1 to Eq. 3 below.

$$\nabla \cdot \boldsymbol{u} = 0 \tag{1}$$

$$\frac{\partial \boldsymbol{u}}{\partial t} + (\boldsymbol{u} \cdot \nabla)\boldsymbol{u} = -\frac{1}{\rho}\nabla P + \upsilon \nabla^2 \boldsymbol{u} + \beta \boldsymbol{g} T' \tag{2}$$

$$\frac{\partial T'}{\partial t} + (\boldsymbol{u} \cdot \nabla) T' + \gamma u_z = \alpha \nabla^2 T' \tag{3}$$

where $\boldsymbol{u}$, ρ, P, υ, α, β, $\boldsymbol{g}$, and T' respectively denote velocity, density, pressure, kinematic viscosity, thermal diffusivity, volume expansion coefficient, gravitational acceleration, and temperature fluctuation. Moreover, u_z represents the vertical component of the fluid velocity, while γ $(= dT_b/dz)$ denotes the constant background temperature gradient.

Thermocline Model

In this paper, the density is set as a polynomial function of temperature. The linear stratification of the density is achieved by setting the temperature to vary with the depth direction. The expressions for the temperature T and the density are shown as Eqs. 4 and 5, where T_0 and $\rho_0$are the reference values, and z is the vertical depth with the positive value above the free surface.

$$T(z) = T_0 + c_1 \cdot z \tag{4}$$

$$\rho(z) = \rho_0 - c_2 \cdot z \tag{5}$$

Linear stratified fluids can be realized by coupling Eqs. 1–5. For homogeneous and strongly stratified fluids, c_1 and c_2 are set to zero, and the temperature is treated as a constant.

Turbulence Modeling

To keep the equations closed, the SST k-ω turbulence model is chosen for the solution, and the transport equations for k and ω are given by Eq. 6 and Eq. 7.

$$\frac{\partial}{\partial t}(\rho k) + \frac{\partial}{\partial x_i}(\rho k u_i) = \frac{\partial}{\partial x_j}\left(\Gamma_k \frac{\partial k}{\partial x_j}\right) + G_k - Y_k + S_k \tag{6}$$

$$\frac{\partial}{\partial t}(\rho \omega) + \frac{\partial}{\partial x_i}(\rho \omega u_i) = \frac{\partial}{\partial x_j}\left(\Gamma_\omega \frac{\partial \omega}{\partial x_j}\right) + G_\omega - Y_\omega + S_\omega \tag{7}$$

where Γ_k, Γ_ω represent the effective diffusivity; G_k, G_ω represent the turbulent kinetic energy, Y_k, Y_ω represent the energy dissipation; and S_k, S_ω represent the source terms (Menter, 1994).

Volume of Fluid Method

In the present numerical simulation, the Volume of Fluid (VOF) method is employed to capture the interface between immiscible fluids. The VOF method deals with the interface problem by calculating the volume fraction $r^{(k)}$ occupied by different fluids in each cell.

$$\frac{\partial r}{\partial t} + \nabla \cdot (r \boldsymbol{u}) = 0 \tag{8}$$

$$r^{(k)} = V^{(k)} / \sum_{k=1}^{n} V^{(k)} \tag{9}$$

To accurately capture the sharp interface in STAR-CCM+, the High-Resolution Interface Capturing scheme is adopted. The interface between the two fluids is defined within the range $0 < r < 1$. Based on the value of the volume fraction r, the location of the interface can be identified.

PI-controller

The sliding mesh method is employed to simulate the propeller rotation. The meshes on both sides of the interface are allowed to slide relative to each other while maintaining flux consistency, and the mesh nodes on either side are not required to coincide (Zhang et al., 2022).

The rotational speed of the submarine propeller at the self-propulsion point is determined by the PI control method, which continuously regulates the propeller speed in response to the deviation between the target and current submarine speeds throughout the numerical iterative solution process. The expression of the PI controller is Eq. 10 (Carrica et al., 2019), where $R(t)$ is the rotational speed at different times, and R_0 is the initial value of the rotational speed. The error is the target speed of the submarine minus the current speed. K_p is the proportional gain, which amplifies the instantaneous error and provides a stronger corrective action for larger deviations. K_i is the integral gain, which amplifies the accumulated error of speed over time, thereby eliminating steady-state errors.

$$R(t) = R_0\left(1 + K_p \cdot error + K_i \cdot \sum error\right) \tag{10}$$

COMPUTATIONAL SETUP AND VALIDATIONS

Joubert BB2 Submarine Model

The geometric object studied in this paper is the Joubert BB2, a generic submarine designed by Joubert and adapted by MARIN in the Netherlands. The geometry is shown in Fig. 1, and the main parameters are shown in Table 1.

Computational Domain and Discretized Mesh

This study adopts a computational domain that follows the motion of the submarine, significantly reducing the length of the

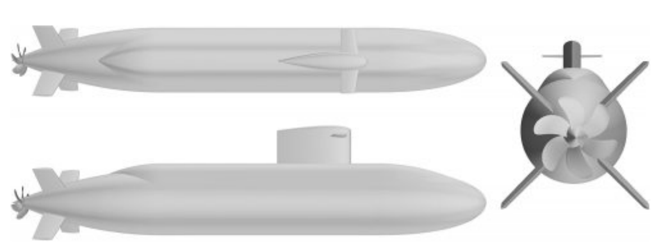

Fig. 1 Joubert BB2 geometry

Parameters	Symbol	Value (m)
Overall length	L	3.826
Beam	B	0.523
Draft to deck	D_d	0.578
Draft to sail top	D_s	0.883
Diameter of propeller	D_p	0.273

Table 1 Main parameters of the Joubert BB2 (model scale 1:18.348)

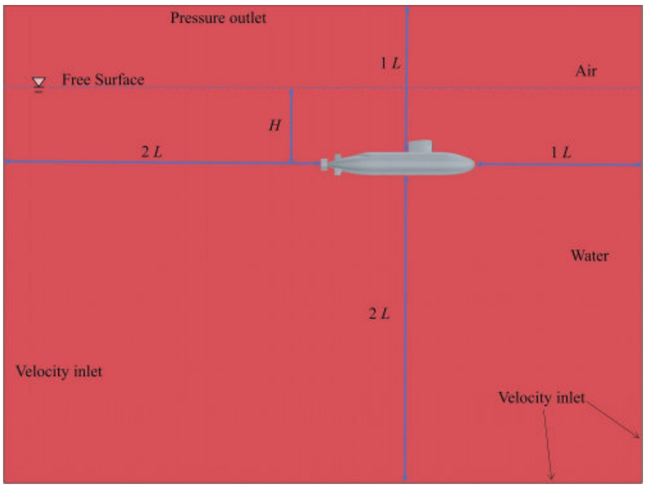

Fig. 2 Computational domain and boundary conditions

computational domain compared to traditional methods. The total length of the computational domain is $4L$, with $1L$ in front of the submarine, $2L$ behind it, and $2L$ on each side. The top boundary of the computational domain is set as a pressure outlet, while all other boundaries are configured as velocity inlets, as shown in Fig. 2.

The trimmed cell mesh was used to discretize the computational domain, with mesh refinement applied near the free surface region and around the propeller. Boundary layer meshes were added on the submarine surface to capture near-wall flow phenomena. To ensure numerical stability during propeller rotation, a small clearance of approximately 5 mm was introduced at the junction between the hub and the hull, serving as the interface between the rotating and non-rotating domains. The final mesh consists of approximately 16 million cells. The mesh results are shown in Fig. 3.

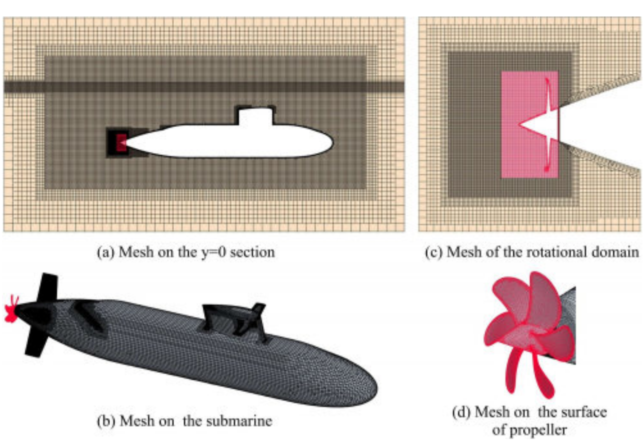

Fig. 3 Mesh details for the domain

Mesh case	Cells (million)	Rotational speed (rpm)	ε_1 (%)	Thrust (N)	ε_2 (%)
1	5.7	282	−1.78	27.08	−5.12
2	12	285.5	−0.56	27.71	−2.91
3	16	288.4	0.45	29.05	1.79
4	26	287.1	—	28.54	—

Table 2 Results of mesh convergence

An implicit first-order unsteady scheme is employed for time discretization, while a second-order upwind method is used for spatial discretization. The pressure–velocity coupling is handled using the segregated flow solver. The time step is set to 0.01 s.

Mesh Convergence Analysis

A mesh convergence analysis was conducted for the self-propulsion case at a submergence depth of $0.21L$ and an advancing speed of 1.2 m/s. The water density was set to 997.56 kg/m^3, and four grid resolutions with total cell counts of 5.7, 12, 16, and 26 million were used. In all four mesh configurations, the same refinement strategy was applied, with only the grid size being varied. The propeller rotational speed and thrust obtained at the self-propulsion point for each grid are summarized in Table 2, where the rotating speed was determined by a PI controller.

As shown in Table 2, the deviation from the results obtained with the finest grid decreases as the grid resolution increases. When the grid size is increased from 16 million to 26 million cells, the variations in both the propeller rotational speed and thrust at the self-propulsion point remain within 2%. Therefore, to balance computational cost and numerical accuracy, a grid with 16 million cells was adopted for the present simulations.

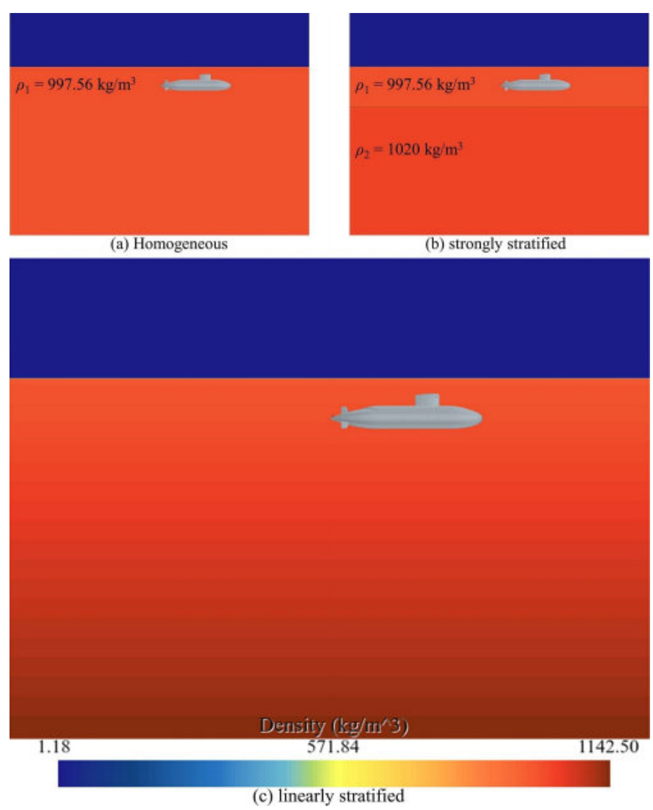

Fig. 4 Initial density fields for the three kinds of fluids

Initial Density Fields for Stratified Simulation

In this paper, the density at the center of mass of the submarine is uniformly set to 997.56 kg/m^3, and the position of the free surface H determines the interface between air and water. When the fluid is strongly stratified, the region $0.32L$ below the center of mass of the submarine is set to be heavy-density fluid with a density of 1,020 kg/m^3. The coefficients c_1, c_2 (in Eqs. 4 and 5) are 1.5 and 18.3, respectively, when the fluid is continuously stratified. The density fields of the three kinds of fluid at the initial moment are shown in Fig. 4.

Numerical Verification and Validation

To verify the reliability of the submarine's self-propulsion results in the homogeneous fluid, the experimental results under deep-water conditions from Overpelt et al. (2015) were used for comparison. The results are shown in Table 3.

Table 3 presents the comparison of propeller rotational speed and thrust between the current numerical results and the experimental results of Overpelt et al. (2015). Due to methodological differences, certain discrepancies exist between the numerical results and the experimental data. The error in propeller rotational speed is only 1.49%, and the error in thrust is still within 7%. Therefore, the numerical method used in this study is reliable for submarine self-propulsion simulations.

The validation of the surface waves generated by a body moving at a constant speed in the strongly stratified fluid is shown in Fig. 5, together with the corresponding experimental data (Min et al., 2023). The present result, which is also part of our previous work (Gao et al., 2025), indicates that both the wave amplitude and spatial distribution agree well with the experimental measurements, thereby confirming the reliability of the present numerical simulations in strongly stratified conditions.

Since no reference wave elevation data is available in linearly stratified density fields, the verification was performed only for the homogeneous fluid. For consistency, the computational setup followed that of Torunski (Huang et al., 2022). The comparison of free-surface wave elevations is presented in Fig. 6, showing very close agreement between the two results. Moreover, this topic has been systematically investigated and reported in several of our previous studies (Cao et al., 2021, 2023), which provide comprehensive analyses of the wave patterns, propagation characteristics, and underlying physical mechanisms.

Parameters	Present	Experiment	Error
Velocity (m/s)	1.2	1.19	—
Rotating speed (rpm)	272	268	1.49%
Thrust (N)	24.92	26.6	−6.32%

Table 3 Comparison between present and experimental results

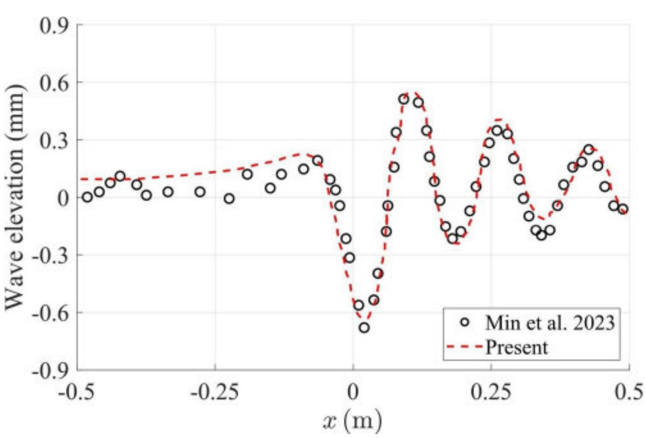

Fig. 5 Validation of surface wave elevation results in strongly stratified fluid

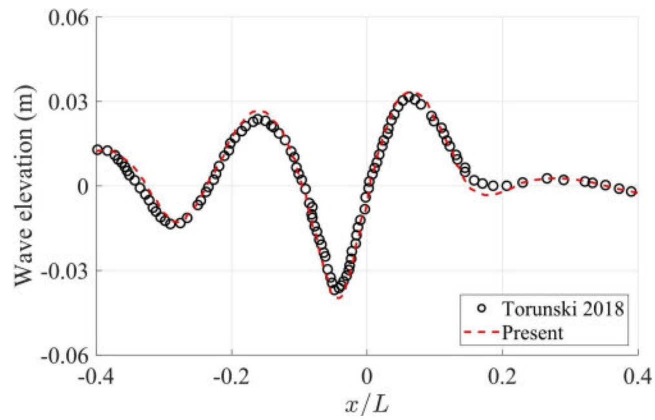

Fig. 6 Verification of surface wave elevation results in homogeneous fluid

RESULTS AND DISCUSSION

Hydrodynamic Results of Self-propulsion

The rotational speeds and thrusts corresponding to the self-propelled points of the Joubert BB2 submarine for the nine conditions considered in this paper are shown in Table 4. The speed of the model scale submarine is 1.2 m/s, which corresponds to 10 kn in the full scale, and the submerged depths include 0.17, 0.21, and $0.26L$. The density stratification of the fluid is divided into three categories, which are homogeneous density fluid, strongly stratified fluid, and linearly continuous stratified fluid.

From Table 4, it can be observed that both the rotational speed of the propeller and the generated thrust decrease as the diving depth increases. This trend arises from the decrease in wave-making resistance at greater submergence depths, where the influence of surface-generated waves becomes weaker, thus lowering the propulsion demand. Furthermore, under the same dive depth, the differences in rotational speed and thrust between the two types of stratified fluids and the homogeneous density fluid remain within 3%. This minor variation suggests that, when operating near the surface in a self-propelled state, the influence of density stratification on the propulsive performance of the submarine is very small.

Case	Depth/L	Fluid	Rotational speed (rpm)	Thrust (N)
1		homogeneous	320.7	39.23
2	0.17	strongly stratified	315.2	39.39
3		linearly stratified	316.7	39.35
4		homogeneous	288.4	29.05
5	0.21	strongly stratified	281.4	29.89
6		linearly stratified	283.9	29.78
7		homogeneous	280.8	26.64
8	0.26	strongly stratified	277.6	26.67
9		linearly stratified	278.3	26.98

Table 4 Rotational speed and thrust results for nine cases

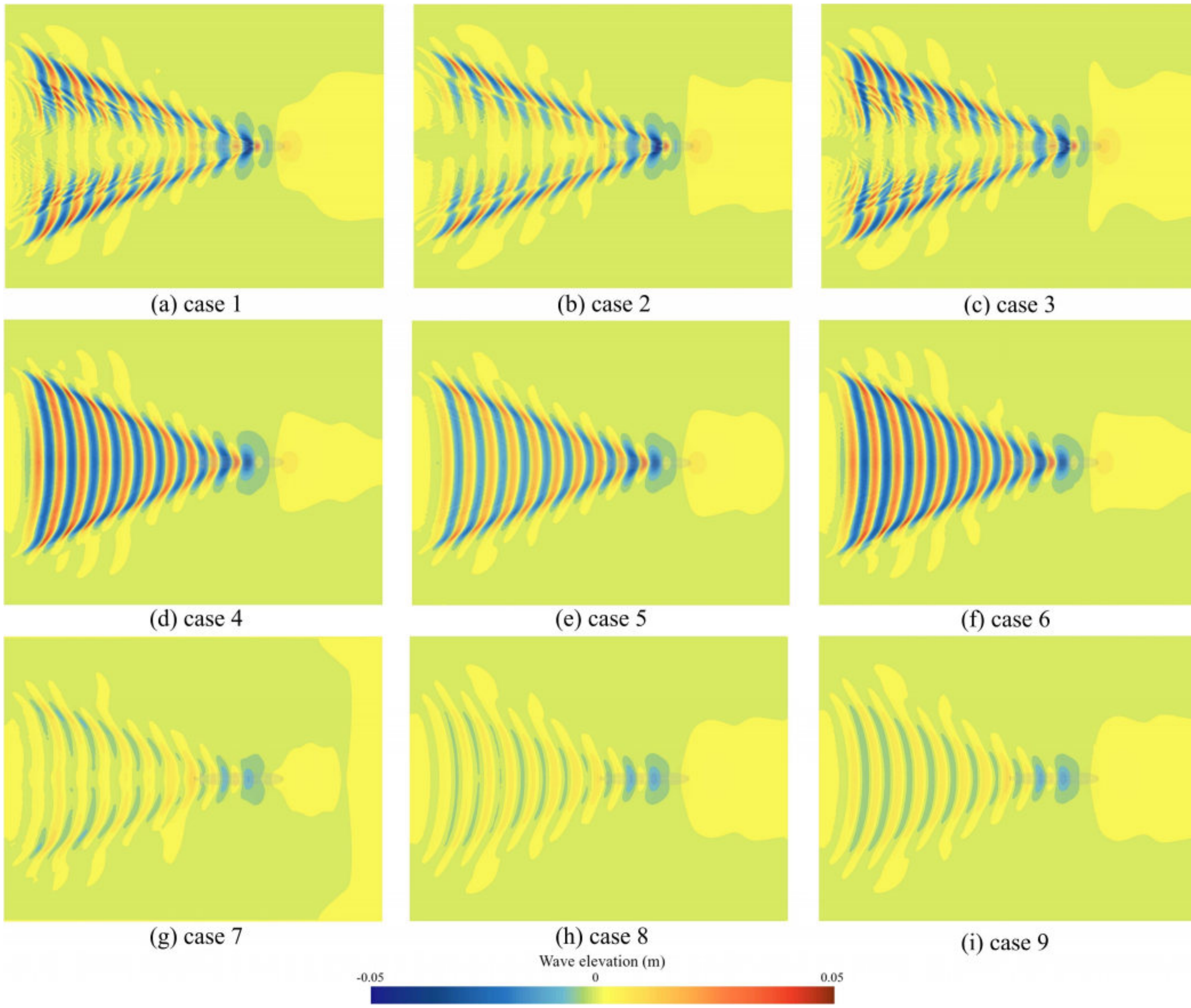

Fig. 7 Free surface wave shapes for nine cases

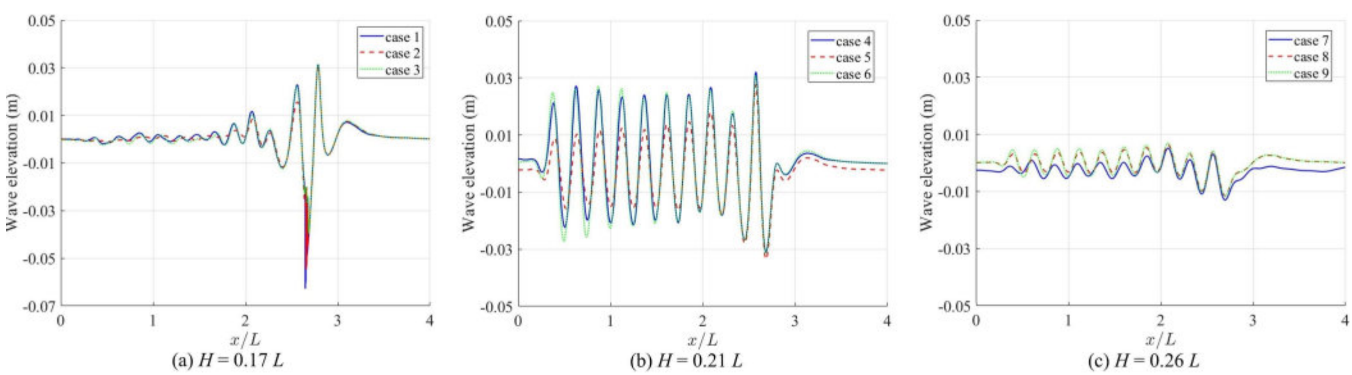

Fig. 8 Surface wave elevations for nine cases

Free Surface Waves

Similar to the wave system generated by a ship, a submarine operating under self-propulsion in close proximity to the free surface produces a Kelvin-like wave pattern on the water surface. This phenomenon arises from the disturbance caused by the submerged body moving through the fluid, which propagates upward and interacts with the surface. The resulting surface wave patterns corresponding to nine representative cases are illustrated in Fig. 7, providing a clear visualization of the surface disturbances. In addition, Fig. 8 presents the variations in wave elevation along the submarine's longitudinal profile, offering a more detailed perspective on the wave distribution characteristics influenced by depth and stratification conditions. It should be noted that at a submer-

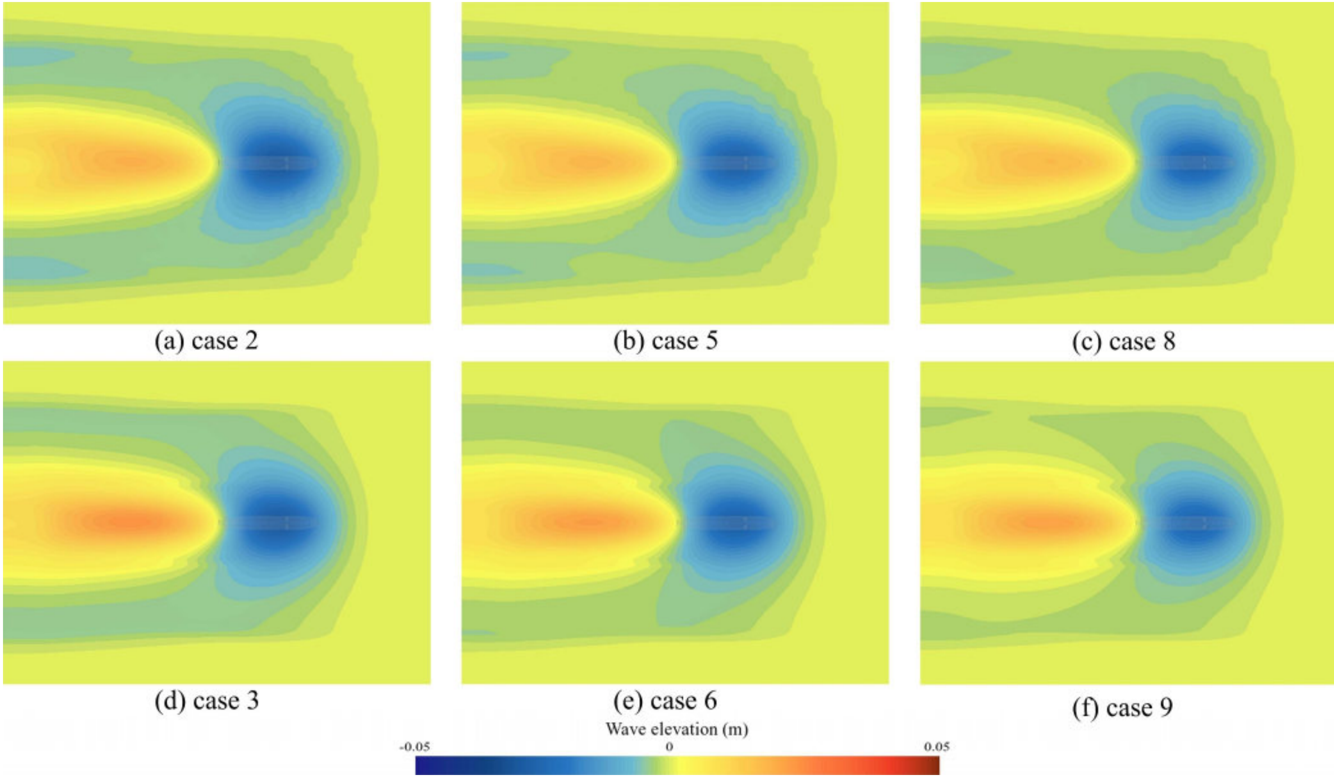

Fig. 9 Internal wave shapes for six cases

gence depth of $0.17L$, the sail of the submarine is very close to the free surface, which leads to a sharp and localized drop in the wave trough at $x/L \approx 2.65$, as shown in Fig. 8a.

From Figs. 7a–7c and Fig. 8a, it can be clearly observed that when the submarine operates at a shallow depth of $0.17L$ below the free surface, the resulting surface wave patterns and corresponding wave elevation distributions exhibit remarkable similarity across all three fluid conditions—namely, homogeneous, strongly stratified, and linearly stratified fluids. This consistency suggests that, under such near-surface operating conditions, the influence of density stratification on the surface waves generated by the self-propulsion of the submarine is negligible.

Figures 7d–7f and Fig. 8b show that when the submarine's depth increases to $0.21L$ below the free surface, the overall surface wave patterns remain nearly identical among the three fluid conditions, indicating that the general structure of the wave field is not significantly affected by the stratification at this depth. However, a closer examination of the wave elevation data reveals that the amplitude of the surface waves in the strongly stratified fluid is slightly lower than that of those observed in the homogeneous and linearly stratified fluids.

Figures 7g–7i and Fig. 8c reveal that at a depth of $0.26L$ beneath the free surface, the differences in surface wave patterns among the three fluid conditions become most pronounced. In particular, the surface waves generated in the homogeneous fluid appear less developed and less continuous compared to those observed in the strongly and linearly stratified cases. This is especially evident in the wave elevation distribution along the submarine's centerline, where the homogeneous case exhibits a markedly lower amplitude. These results indicate that density stratification enhances the transmission of disturbance energy from the submerged body to the free surface, leading to more complete and higher-amplitude wave formations in stratified fluids.

Internal Waves

When a submarine operates under self-propulsion in a density-stratified fluid, it generates not only surface waves but also internal waves. In strongly stratified fluids, the internal waves are located at the interface between the two density layers. For comparative analysis, the internal waves in continuously stratified fluids are represented by the iso-surface where the density is 1,020 kg/m^3. The internal wave patterns for six density stratification conditions are shown in Fig. 9, while the wave elevation results along the submarine's longitudinal profile are presented in Fig. 10.

From Fig. 9, it can be observed that for the Joubert BB2 submarine model moving at a constant speed of 1.2 m/s above the internal density interface, the resulting internal wave patterns exhibit a consistent structure across all examined cases. Specifically, a

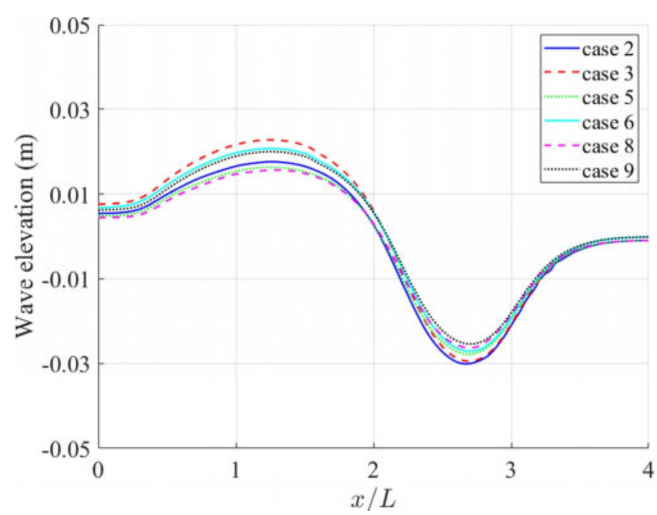

Fig. 10 Internal wave elevations for six cases

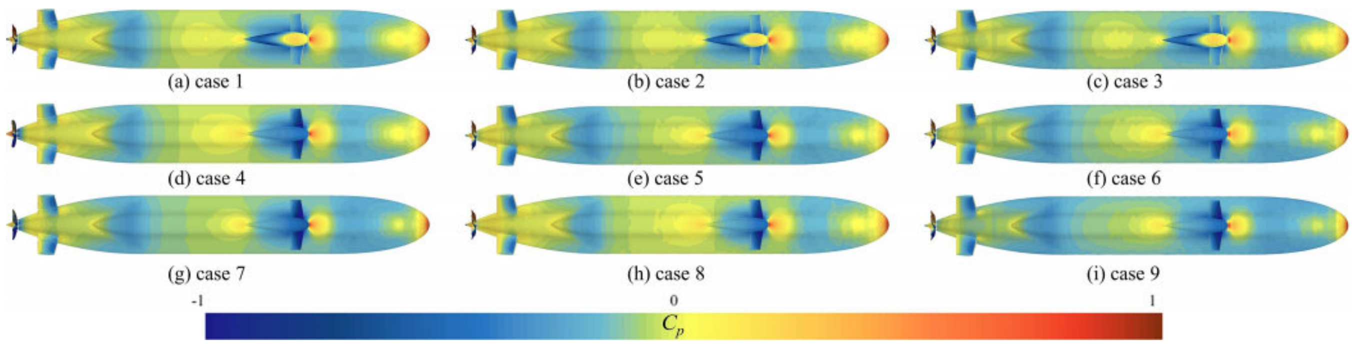

Fig. 11 Pressure distribution on the upper surface of the submarine

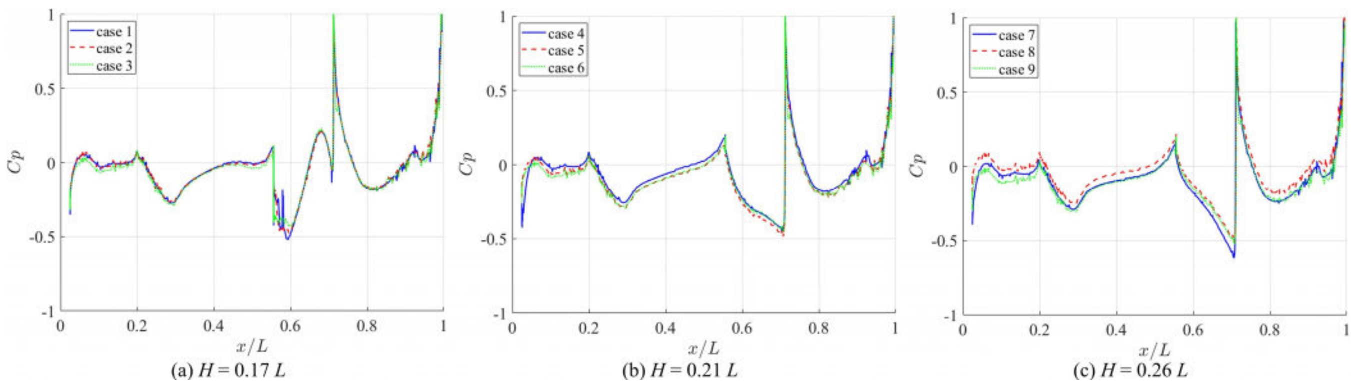

Fig. 12 Pressure coefficient along the longitudinal section of the submarine's upper surface

pronounced trough is generated directly beneath the submarine, while a crest forms in its wake. This wave pattern reflects the typical response of a stratified fluid to the passage of a submerged body, where the vertical displacement of the internal interface is governed by the interaction between the body-induced disturbance and the buoyancy stratification. The persistent appearance of this trough-crest pattern indicates a stable and repeatable internal wave generation mechanism under these flow conditions.

Figure 10 reveals that when the vertical distance between the submarine and the internal density interface is kept constant, the amplitudes of the internal waves—both crest and trough—become more pronounced as the submarine operates closer to the free surface. This indicates that the surface proximity enhances the strength of the disturbance transmitted to the internal interface, leading to greater vertical displacements. Furthermore, a comparison between different stratification conditions shows that under the strongly stratified fluid, the internal wave trough exhibits slightly larger values than those observed under the continuously (linearly) stratified condition, whereas the crest values are marginally higher in the linearly stratified fluid. These subtle differences suggest that the stratification profile influences the asymmetry and distribution of internal wave energy, potentially due to variations in the restoring buoyancy force and wave dispersion characteristics between the two stratification types.

Pressure Coefficients

Figures 11 and 13 show the pressure coefficient results on the upper and lower surfaces of the self-propelled submarine for nine cases. Figures 12 and 14 present the pressure coefficient distributions along the centerline of the upper and lower surfaces, respectively. The expression for the pressure coefficient is Eq. 11. In the homogeneous and strongly stratified fluids, ρ_h is 997.56 kg/m^3. In the linearly stratified fluid, ρ_h varies with depth.

$$C_p = (P - P_h)/(\tfrac{1}{2}\rho_h U^2) \tag{11}$$

From Figs. 11–14, it can be clearly observed that, under the same submerged depth conditions, the influence of strongly density-stratified fluid on the pressure coefficient distribution along the upper and lower surfaces of the submarine is relatively small. Specifically, the pressure coefficients on both the upper and lower surfaces exhibit only minor deviations from those observed in the homogeneous fluid, indicating that strong density stratification does not substantially alter the pressure field around the vehicle. In contrast, when the surrounding fluid exhibits a linear density stratification, the effect on the pressure coefficient becomes more asymmetric. While the upper surface still shows relatively small changes, similar to the strongly stratified and uniform cases, the lower surface demonstrates a notable increase in pressure coefficient values. This suggests that linear density stratification leads to a more pronounced disturbance of the flow field beneath the submarine, with the linear density gradient interacting with the downward flow and consequently producing higher pressure levels than those under homogeneous conditions.

Velocity Field and Density Fluctuation

To investigate the underlying reasons for the significant differences observed in the surface wave patterns generated by the submarine's self-propulsion at a depth of $0.26L$ across the three types of fluids, an analysis of the velocity field was carried out for this specific submergence depth condition. This analysis aimed to reveal how variations in fluid stratification influence the flow characteristics near the submarine and, consequently, the energy transmitted to the free surface. The resulting horizontal and vertical velocity components along the submarine's longitudinal profile are presented in Fig. 15.

It can be observed from Fig. 15 that when the submarine is in a uniform fluid, the horizontal and vertical velocity fields behind the propeller exhibit an upward motion toward the water surface. However, this upward trend is absent in the strongly stratified and linearly stratified fluids, which explains the differences in the

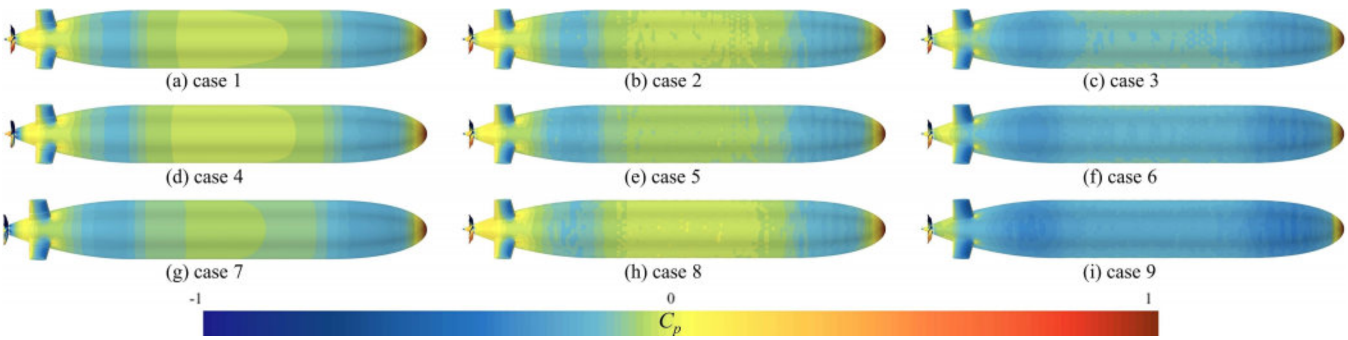

Fig. 13 Pressure distribution on the lower surface of the submarine

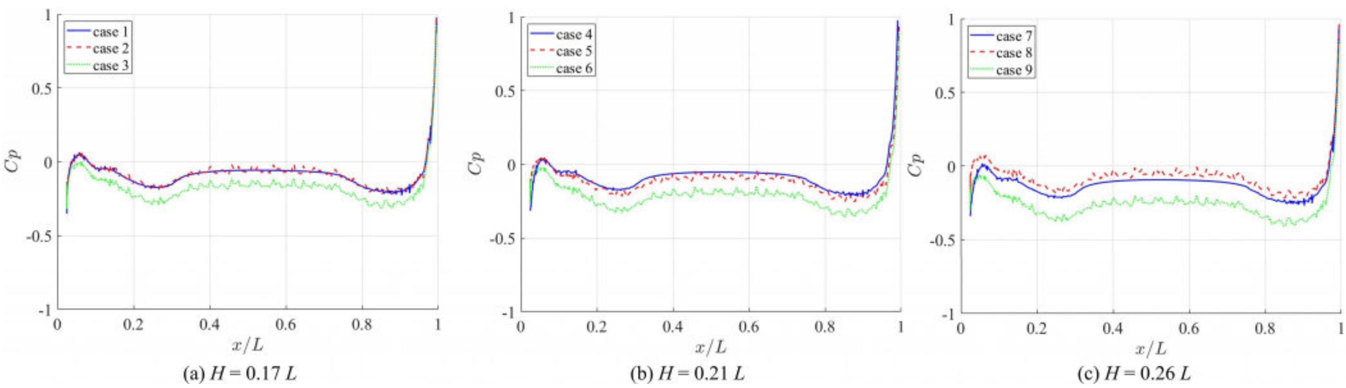

Fig. 14 Pressure coefficient along the longitudinal section of the submarine's lower surface

surface wave results shown in Figs. 6g–6i. This is consistent with the findings of More and Ardekani (2023), who reported that in density stratified fluids, the density gradient inhibits fluid motion in the vertical direction, compared to that in a homogeneous fluid where the wake is more likely to spread vertically.

In addition, as shown in Fig. 16, the suction effect induced by the propeller leads to noticeable mixing and oscillation of fluid layers with different densities in the wake region within the

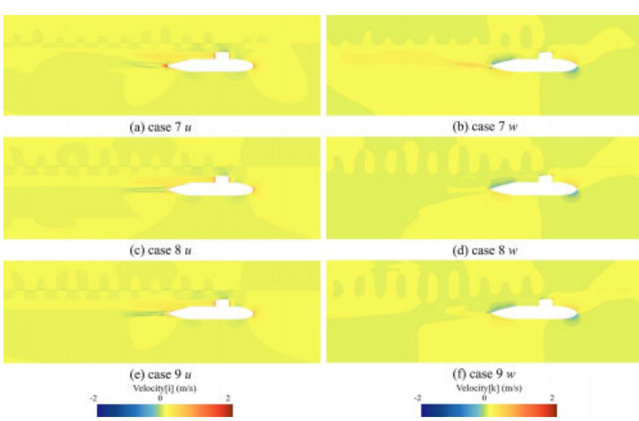

Fig. 15 Velocity field at the submergence depth of $0.26L$

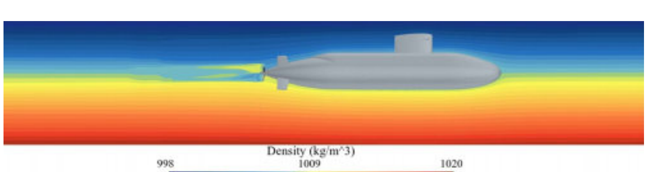

Fig. 16 Density field in the wake region of the linear stratified fluid

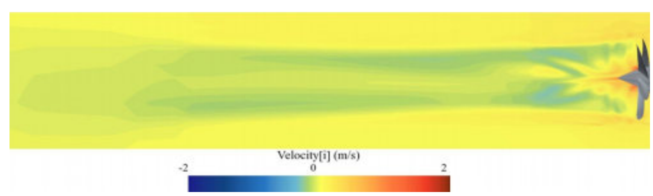

Fig. 17 Horizontal velocity field in the wake region of the linearly stratified fluid

linearly stratified fluid. This dynamic interaction results in low-density fluid being drawn upward, while high-density fluid tends to sink, creating localized vertical displacements in the wake. Consequently, a convergence of horizontal velocity toward the propeller axis is observed over a certain downstream distance. This flow behavior is clearly illustrated in Fig. 17, where the streamwise velocity field demonstrates a narrowing of the wake structure. Such convergence is indicative of the stratification-driven constraint on vertical mixing, which modifies the momentum distribution in the wake and reflects the complex coupling between stratification effects and propeller-induced flow structures.

To quantitatively investigate the influence of density stratification on the flow-field structure in the submarine wake, the vertical velocity at one submarine length downstream along the axis was analyzed, as shown in Fig. 18. The results indicate that when the submarine advances at a self-propulsion speed of 1.2 m/s at a submergence depth of 0.26L below the free surface, the maximum absolute vertical velocities in the three density environments are 0.747 m/s, 0.458 m/s, and 0.284 m/s, respectively. In the strongly stratified and continuously stratified conditions, the absolute vertical velocity decreases by 38.7% and 61.9%, respectively, compared with the homogeneous fluid. In addition, the velocity direction reveals that within $0.2L$ downstream of the submarine, the fluid moves downward in the continuously stratified environment,

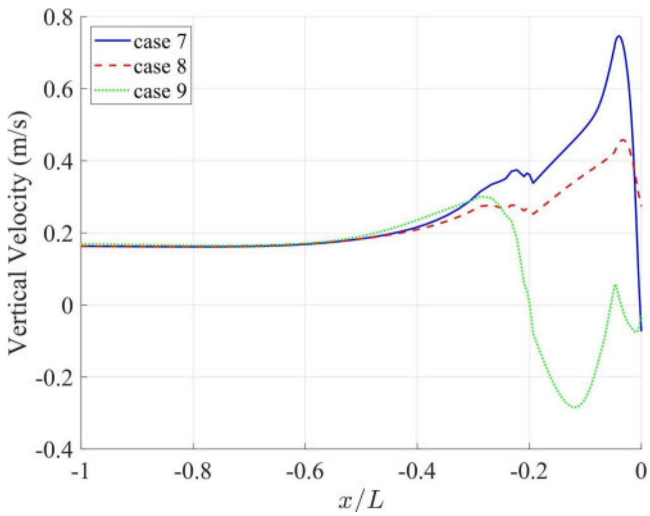

Fig. 18 Vertical velocity within one submarine length downstream along the submarine axis

whereas it moves upward in the homogeneous and strongly stratified fluids. The effect of density stratification is limited in extent and beyond $0.5L$ downstream, the vertical velocities in all three fluid environments become nearly identical.

In summary, the comparative analysis of the velocity field and density fluctuations demonstrates that density stratification constrains the vertical motion of fluid particles in the submarine wake. This effect reduces the vertical velocity amplitude, alters the wake convergence pattern, and induces local mixing of the density layers, all of which fundamentally reshape the momentum distribution in the near-wake region.

CONCLUSIONS

This study carried out numerical simulations of the BB2 submarine model operating near the free surface under self-propulsion at a speed of 1.2 m/s in three different fluid environments: homogeneous fluid, strongly stratified fluid, and linearly stratified fluid. Simulations were performed for three different depths, resulting in a total of nine cases, to analyze the effects of density stratification on the flow field of a near-surface self-propelled submarine. The main findings are summarized as follows:

1. When the submarine operates near the free surface under self-propulsion, the propeller rotational speed and thrust exhibit very small variations when comparing strongly stratified and linearly stratified fluid environments with the homogeneous fluid case. This indicates that the presence of density stratification—whether strong or linear—has limited impact on the submarine's propulsion performance in terms of these key parameters under near-surface operating conditions.

2. If the submarine operates at a very shallow depth, such as in the $0.17L$ case calculated in this study, the surface wave results generated by self-propulsion are almost identical across the three kinds of fluids. However, as the depth increases, the differences become more pronounced. At a depth of $0.26L$, the wave shape in the homogeneous fluid is not as pronounced as that in stratified environments, and the wave elevation along the submarine's longitudinal profile is significantly lower.

3. Regarding the pressure coefficient distribution on the submarine's surface, the values on the lower surface of the submarine are notably higher in the linearly stratified fluid compared to those in both the homogeneous fluid and the strongly stratified fluid. This suggests that linear density stratification exerts a more pronounced influence on the pressure field beneath the submarine, owing to the gradual density gradient, which affects the flow dynamics differently from homogeneous or strongly stratified conditions.

4. When the submergence depth increases to $0.26L$, density stratification in both strongly and linearly stratified fluids significantly suppresses the vertical motion in the submarine wake, leading to reductions of 38.7% and 61.9% in vertical velocity amplitude compared with the homogeneous fluid, and altering the convergence characteristics of the wake. In the near-wake region, the momentum distribution is markedly reshaped, thereby explaining the differences in free-surface fluctuations under the three different density-stratified environments.

ACKNOWLEDGEMENTS

This work is supported by the National Natural Science Foundation of China (Grant Nos. 52001210, 52131102), to which the authors are most grateful.

REFERENCES

Amiri, MM, Esperança, PT, Vitola, MA, and Sphaier, SH (2018). "How Does the Free Surface Affect the Hydrodynamics of a Shallowly Submerged Submarine," *Appl Ocean Res*, 76, 34–50. https://doi.org/10.1016/j.apor.2018.04.008.

Cao, LS, Gao, G, Guo, EK, and Wan, DC (2023). "Hydrodynamic Performances and Wakes Induced by a Generic Submarine Operating near the Free Surface in Continuously Stratified Fluid," *J Hydrodyn*, 35(3), 396–406. https://doi.org/10.1007/s42241-023-0037-8.

Cao, LS, Huang, FL, Liu, C, and Wan, DC (2021). "Vortical Structures and Wakes of a Sphere in Homogeneous and Density Stratified Fluid," *J Hydrodyn*, 33(2), 207–215. https://doi.org/10.1007/s42241-021-0032-x.

Carrica, PM, Kim, Y, and Martin, JE (2019). "Near-Surface Self Propulsion of a Generic Submarine in Calm Water and Waves," *Ocean Eng*, 183, 87–105. https://doi.org/10.1016/j.oceaneng.2019.04.082.

Chase, N, and Carrica, PM (2013). "Submarine Propeller Computations and Application to Self-Propulsion of DARPA Suboff," *Ocean Eng*, 60, 68–80. https://doi.org/10.1016/j.oceaneng.2012.12.029.

Dong, K, Wang, X, Zhang, D, Liu, L, and Feng, D (2022). "CFD Research on the Hydrodynamic Performance of Submarine Sailing near the Free Surface with Long-Crested Waves," *J Mar Sci Eng*, 10(1), 90. https://doi.org/10.3390/jmse10010090.

Gao, G, Cao, LS, Wan, DC, and Zhu, J (2025). "Numerical Investigations of Wake Flows of an Underwater Vehicle near Free Surface in Two-Layer Fluids," *Int J Offshore Polar Eng*, ISOPE, 35(3), 289–299. https://doi.org/10.17736/ijope.2025.ak75.

Guo, EK, Wang, YJ, Cao, LS, and Wan, DC (2024). "Numerical Investigation on Steady Turning Motion of a Generic Submarine near the Free Surface," *Ocean Eng*, 313, 119375. https://doi.org/10.1016/j.oceaneng.2024.119375.

Huang, FL, Meng, QJ, Cao, LS, and Wan, DC (2022). "Wakes and Free Surface Signatures of a Generic Submarine in the Homogeneous and Linearly Stratified Fluid," *Ocean Eng*, 250, 111062. https://doi.org/10.1016/j.oceaneng.2022.111062.

Li, Y, Martin, E, Michael, T, and Carrica, PM (2015). "A Study of Propeller Operation near a Free Surface," *J Ship Res*, 59(4), 190–200. https://doi.org/10.5957/jsr.2015.59.3.190.

Liefvendahl, M, and Troëng, C (2011). "Computation of Cycle-To-Cycle Variation in Blade Load for a Submarine Propeller Using LES," *Proc 2nd Int Symp Mar Propulsors*, Hamburg, Germany, SMP11, 1–7.

Lungu, A (2022). "A DES-based Study of the Flow Around the Self-propelled DARPA Suboff Working in Deep Immersion and Beneath the Free-Surface," *Ocean Eng*, 244, 110358. https://doi.org/10.1016/j.oceaneng.2021.110358.

Ma, WZ, Li, Y, Ding, Y, Duan, F, and Hu, KY (2020). "Numerical Investigation of Internal Wave and Free Surface Wave Induced by the DARPA Suboff Moving in a Strongly Stratified Fluid," *Ships Offshore Struct*, 15(6), 587–604. https://doi.org/10.1080/17445302.2019.1661633.

Menter, FR (1994). "Two-equation Eddy-Viscosity Turbulence Models for Engineering Applications," *AIAA J*, 32(8), 1598–1605. https://doi.org/10.2514/3.12149.

Min, EH, et al. (2023). "Experimental and Numerical Study on Wave Characteristics by a Moving Submerged Body in a Two-Layer Fluid," *Ocean Eng*, 281, 114979. https://doi.org/10.1016/j.oceaneng.2023.114979.

More, RV, and Ardekani, AM (2023). "Motion in Stratified Fluids," *Annu Rev Fluid Mech*, 55(1), 157–192. https://doi.org/10.1146/annurev-fluid-120720-011132.

Overpelt, B, Nienhuis, B, and Anderson, B (2015). "Free Running Manoeuvring Model Tests on a Modern Generic SSK Class Submarine (BB2)," *Pac Int Marit Conf*, Sydney, Australia, MARIN, 1–14.

Sezen, S, Dogrul, A, Delen, C, and Bal, S (2018). "Investigation of Self-Propulsion of DARPA Suboff by RANS Method," *Ocean Eng*, 150, 258–271. https://doi.org/10.1016/j.oceaneng.2017.12.051.

Sudharsun, G, et al. (2022). "Free Surface Features of Submarines Moving Underwater: Study of Bernoulli Hump," *Ocean Eng*, 249, 110792. https://doi.org/10.1016/j.oceaneng.2022.110792.

Torunski, B (2018). *Computational Analysis of The Free Surface Effects on a BB2 Submarine Undergoing Horizontal Maneuvers*, University of New Brunswick, 60–95.

Zhang, DP, Yan, J, Zhao, BW, Zhu, KQ, and Hou, L (2022). "Numerical Simulation and Analysis of Propeller's Open Water Performance," *Ship Standard Eng*, 55(4), 27–37 (in Chinese). https://doi.org/10.14141/j.31-1981.2022.04.0066.